

# Density functional theory study of Na at Al(111) and O at Ru (0001)

C. Stampfl

*Fritz-Haber-Institut der Max-Planck-Gesellschaft*

*Faradayweg 4-6, D-14 195 Berlin-Dahlem, Germany*

## Abstract

The success of density functional theory for the description of the adsorption of atoms on surfaces is well established, and based on recent calculations using gradient corrections, it has been shown that it also describes well the dissociative adsorption of molecules at surfaces – admittedly however, the data base for reactions at surfaces is still somewhat small. In the present paper the power of density functional theory calculations is demonstrated by investigations for two different adsorption systems, namely, one with a strongly electropositive adsorbate [Na on Al(111)] and one with a strongly electronegative adsorbate [O on Ru(0001)]. In each case, new hitherto not expected adsorbate phases have been predicted by the theory: For Na on Al(111) the stability of a “four-layer” surface alloy was identified while for O on Ru(0001) it was predicted that the formation of a  $(1 \times 1)$ -O adlayer should be possible which implies that the apparent saturation coverage of  $\Theta_{\text{O}} = 1/2$  is due to kinetic hindering.

## I. INTRODUCTION

It is of great interest to have an accurate theoretical framework for the description of the interaction and reaction of particles at surfaces. Calculations of this nature would give insight and understanding into the varied and complex processes that take place between atoms, molecules, and solid surfaces. In relation to this, information concerning atomic and electronic structure, energy barriers, site specificity, bond formation and scission, and the identification of reaction pathways could be obtained. Indeed, experimentally, a strong motivation for chemisorption studies with well-defined single crystal surfaces is the prospect of gaining deeper insight into the elementary steps governing heterogeneously catalyzed reactions. Obviously a proper theoretical description of such processes at surfaces with accurate predictive power is of enormous technological importance, particularly for example, in the field of catalysis. In this respect, density functional theory is emerging as a very promising approach for describing these phenomena which involve the breaking and formation of chemical bonds, as for example, in the cases of dissociative adsorption, associative desorption, and chemical reactions.

Many first-principles theoretical calculations have been performed for atoms, molecules, and small clusters using quantum chemical methods [1], and for bulk crystals, clean surfaces, and surfaces with adsorbates using methods originating from solid state physics [2]. Far fewer, however, have been performed for systems containing both, that is, atoms and molecules at or above surfaces, as for example, gas-surface systems, or for chemical reactions at surfaces. Thus, schemes for performing calculations for these kinds of systems typically employ either a finite cluster of atoms or a supercell geometry, reflecting the respective approaches of chemists and physicists. The supercell method in particular, is proving to be a very successful method for these kinds of problems even though its application to such systems represents a relatively new field. See, for example, the recent studies of hydrogen dissociation at various surfaces in Refs. [3–8].

From studies performed over the last few years, it has been demonstrated that an im-

proved description of the exchange and correlation energy functional is necessary for a realistic description of the physical and chemical properties of certain systems. The presently most successful and widely used approach of achieving this is to use the generalized gradient approximation (GGA). Such an approach results in a significantly improved description of free atoms and molecules, see for example, [9–12]. Also for the calculation of hydrogen dissociation, where bonds are in the process of being broken and reformed, the GGA has been found to be of crucial importance for obtaining energy barriers in agreement with experiment. Cohesive [13] and chemisorption energies obtained using the GGA are also found to be considerably closer to experiment than the LDA values, for example, molecules at surfaces in which there are strong charge inhomogeneities in the system, e.g., for CO adsorption [14,15]. We note that improvement brought about by using the GGA is not limited to atoms and molecules in free space and at surfaces, it has also been found, for example, in a study for different phases of ice to be necessary in order to describe the hydrogen bond properly [16]. Furthermore, it has been shown to improve the coexistence pressure for the diamond structure to  $\beta$ -tin phase transition in Si [17] and in describing a high-pressure phase transition of SiO<sub>2</sub> [18]. There is still some difficulty in treating certain systems however, as highlighted recently in a test of twenty-four different local and gradient-corrected DFT methods [19] for the energy barrier of the  $\text{H} + \text{H}_2 \longrightarrow \text{H}_2 + \text{H}$  reaction. In this study it was found that the energy barrier is significantly underestimated when using the LDA *or* a GGA. In this case, inclusion of a self-interaction correction (SIC) was found to be important.

For surfaces, however, numerous calculations have demonstrated that DFT within the LDA represents a good description of the quantum-mechanical many-body interactions for well-bonded situations, where calculated electron densities, atomic geometries, and total energy differences are very reliable. Nevertheless, the role, of the GGA in calculations for adsorbates at surfaces, including diffusion barriers, is not yet clear.

In the present paper recent results of density functional theory calculations for two quite different adsorption systems are discussed. The first system involves a strongly electropositive adsorbate, namely, sodium on Al(111) for which the stability of an ordered “four-layer”

surface alloy with a  $(2 \times 2)$  periodicity was identified [20]. This structure was recently confirmed by low energy electron diffraction (LEED) intensity and surface extended x-ray adsorption fine structure (SEXAFS) studies [21]. The second system concerns the adsorption of oxygen on Ru(0001) for which it was very recently predicted that the formation of a  $(1 \times 1)$  adlayer should be possible which therefore implies that the apparent saturation coverage of  $\Theta_{\text{O}} = 1/2$  observed under ultra high vacuum conditions using molecular oxygen is due only to kinetic hindering [22].

### A. Calculation method

The calculation method used to study the two adsorption systems is the pseudopotential plane wave method employing *ab initio*, fully separable pseudopotentials where the adsorbate system is modelled using the supercell approach. The calculation scheme [23,24] affords a fully self-consistent relaxation of the electrons and full relaxation of the atomic positions using damped molecular dynamics. Calculations for Na on Al(111) were carried out primarily using the local-density approximation (LDA) for the exchange-correlation functional [25] where the non-linear form of the core-valence exchange-correlation functional was taken into account for the alkali metal atom [23,26]. Further details of the calculation can be found in Ref. [20]. One additional calculation was performed for the identified  $(2 \times 2)$ -Na/Al(111) surface structure using the GGA of Perdew *et al.* [11]. In this respect, we note that the GGA functional is used in creating the pseudopotentials as well as in the surface calculations. Thus the GGA is treated in a consistent way which is to be distinguished from the inconsistent approach where LDA pseudopotentials are used, with an otherwise GGA treatment. For the calculations for O on Ru(0001) we employed the GGA for all calculations because for our later, related work on the catalytic oxidation of carbon monoxide reaction, use of the GGA is expected to be very important. Details of the calculations are given in Ref. [22].

## II. $(2 \times 2)$ -NA/AL (111)

Recent studies of Na and other alkali metal atoms on Al(111) have revealed that these systems contradict almost every expectation of alkali metal adsorption behavior based on traditional understanding (see, for example, Refs. [27–29]). In particular, at room temperature where thermal energy allows activation barriers to be overcome, evidence was presented from a combined surface extended x-ray adsorption fine structure (SEXAFS) and density-functional theory (DFT) study [30] that an unexpected reaction takes place between the Na atoms and the Al atoms at the surface: The Na atoms “kick-out” surface Al atoms and adsorb in their place, occupying surface substitutional sites. The resulting structure has a  $(\sqrt{3} \times \sqrt{3})R30^\circ$  periodicity and a local coverage of  $\Theta = 1/3$ , where  $\Theta$  is the ratio of the number of adsorbate atoms to the number of substrate atoms in an ideal layer. The surface substitutional site for Na was later confirmed by a detailed LEED intensity analysis [31]. In addition to sodium, it was subsequently shown that potassium [32] and rubidium [33] also adsorb substitutionally at room temperature with the same periodicity and coverage. Adsorption of lithium on Al(111) results in a  $(\sqrt{3} \times \sqrt{3})R30^\circ$  structure and it has been proposed that the Li atoms also adsorb substitutionally [34]; this, however, has not been confirmed by a structural analysis. Cesium, on the other hand, forms a  $(2\sqrt{3} \times 2\sqrt{3})R30^\circ$  structure at room temperature and there is indication from high resolution core level spectroscopy (HRCLS) studies [35] that reconstruction of the substrate also takes place, however, the exact atomic geometry of this phase is to date unknown. At higher coverages ( $\Theta = 1/2$ ) of Na on Al(111), in contrast to K, Rb, and Cs where  $\Theta = 1/3$  is the saturation coverage, a  $(2 \times 2)$  structure forms in which there are two Na atoms per surface unit cell. Identification of the precise atomic geometry of this phase had proved somewhat elusive: Early studies by Porteus [36] and Hohlfeld and Horn [37] suggested models that involved unreconstructed Al substrates, namely, in the former study, it was proposed that there were three rotated domains of  $(2 \times 1)$  periodicity, and in the latter study, the model was proposed to be comprised of two Na layers, each with a  $(2 \times 2)$  periodicity. Based on HRCLS it was concluded [38] that

these previous models were incorrect and that a correct model had to include strongly inter-mixed Na/Al layers. From a normal incidence standing x-ray wave-field (NIXSW) study [39] a model was presented involving two layers each of stoichiometry  $\text{NaAl}_2$ , while from a recent scanning tunnelling microscopy (STM) study [40], it was concluded that in the surface unit cell one Na atom occupies a substitutional site and the other Na atom occupies a hollow site. The, then unclear, situation regarding knowledge of the detailed atomic structure of this  $(2 \times 2)$  phase prompted our theoretical study [20]. By performing calculations for a number of possible surface geometries a particularly stable structure was identified. The validity of this structure, which constitutes a binary “four-layer” surface alloy, was confirmed by low energy electron diffraction (LEED) and SEXAFS [21].

### A. Atomic structure

The atomic structure of  $(2 \times 2)$ -Na/Al(111) is shown in Fig. 1. The Al layer containing atoms of the type  $\text{Al}_2$  we refer to as the “vacancy-layer”. The Na atoms,  $\text{Na}_s$  and  $\text{Na}_f$ , occupy substitutional and fcc-hollow sites, respectively, and in between these two Na layers, Al atoms,  $\text{Al}_1$ , are positioned in hcp-hollow sites with respect to the “vacancy-layer”. The structural parameters determined by DFT-LDA, LEED, and SEXAFS are given in Tab. I. It can be seen that the values agree very well; the interlayer spacings obtained by all three methods deviate by at most by  $0.13 \text{ \AA}$ . We note that the SEXAFS analysis could not uniquely determine the surface structure because good fits between experimental and theoretical SEXAFS curves were also obtained for a different structural model, although it definitely excluded the NIXSW- and STM-derived models. The DFT-LDA and LEED results exhibit, in particular, very good agreement: they both identify the presence of small ( $\approx 0.04 \text{ \AA}$ ) lateral displacements of Al atoms in the “vacancy-layer” ( $\text{Al}_2$ ) and the layer beneath it, as well as a small rumpling ( $\approx 0.05 \text{ \AA}$ ) in the two Al layers beneath the “vacancy-layer”.

The calculations for bulk Al using the GGA gave a lattice constant that is slightly larger than that obtained using the LDA: compare  $4.05 \text{ \AA}$  to  $3.98 \text{ \AA}$ , i.e., it is  $0.07 \text{ \AA}$  or 1.83 %

larger. These values can be compared to the experimental Al lattice constant of 4.02 Å [41] (at low temperature). It is a general trend that GGA-determined lattice constants are larger than the LDA-derived values [13,42,43]. The effect of the GGA with respect to the surface structure is found to yield Na-Al bond lengths somewhat longer than the LDA result; the respective average Na-Al bond lengths are 3.35 Å and 3.26 Å, i.e. the value determined using the GGA is 2.7 % longer than the result obtained using the LDA. For comparison, the corresponding value obtained from the LEED intensity analysis is 3.34 Å which agrees more closely with the GGA result. The bond length of the Al atom, Al<sub>1</sub>, to its nearest neighbors in the “vacancy layer” however, increases by only 0.7 % when using the GGA as compared to the LDA result. With respect to the above-mentioned lateral relaxations, and the rumpling in Al layers five and six (i.e. the first and second Al layers beneath the vacancy-layer, respectively), almost no change is found between the LDA and GGA results. Similarly, the induced work function change is unaltered with a value of −1.16 eV; the value and sign of which reflects the electropositive nature of the Na atom. We note that a similar effect was obtained in calculations for the two ( $\sqrt{3} \times \sqrt{3}$ )-Rb/Al(111) phases which form at low temperature (on-top adsorption site) and room temperature (substitutional adsorption site) [44]. Here the bond lengths obtained for Rb in the on-top and substitutional sites using the LDA were 3.30 Å and 3.65 Å respectively, and using the GGA the corresponding values were 3.45 Å and 3.78 Å. The values obtained from a LEED intensity analysis [33] were 3.34 Å and 3.72 Å respectively, for the on-top and substitutional sites. Similarly, as discussed below, the GGA results for the O-Ru bond lengths are slightly longer than those determined by LEED. The tendency of a GGA to commonly give slightly larger interatomic distances than experiment has been previously noted [11,43], and it appears that this trend extends to bond lengths of adsorbates at surfaces as well.

## B. Mass transport of substrate atoms

The atomic structure of  $(2 \times 2)$ -Na/Al(111) together with that of  $(\sqrt{3} \times \sqrt{3})R30^\circ$ -Na/Al(111), for which Na adsorbs substitutionally, and as mentioned above, likewise is formed for the K and Rb adsorbates, indicates that a certain mass transport occurs on the surface as explained in the following. Considering first the  $(\sqrt{3} \times \sqrt{3})R30^\circ$  structure, it is of interest to consider how it forms and where the “missing”  $1/3$  of a monolayer of Al atoms go. It seems most natural to assume that the alkali metal atoms “kick-out” Al atoms, i.e., a place exchange occurs between the alkali metal atoms and Al atoms in the layer beneath. In relation to this, from DFT calculations [23,30], a mechanism was identified which is necessary for the kick-out reaction process to be significant, namely, the re-bonding of the displaced substrate atoms at kink sites at steps. This uses the fact that in thermal equilibrium kink sites represent the thermodynamic reservoir for substrate atoms and establishes that the chemical potential of the Al atoms equals the cohesive energy. As discussed in Ref. [29], it could also be possible, however, that Al atoms desorb *from* steps and diffuse to the regions between on-surface alkali metal atoms to form the substitutional structure, i.e., the on-surface alkali metal atoms “capture” the Al atoms. Additionally it could be considered that at first the alkali metal atoms kick-out Al atoms which then diffuse to regions between on-surface alkali metal atoms, forming two terraces each with a substitutional structure. Interestingly, from a HRCLS study of the temperature-dependent phase transition from the on-top to substitutional  $(\sqrt{3} \times \sqrt{3})R30^\circ$ -Rb/Al(111) adsorption structures, Al atoms “trapped” between on-surface Rb atoms have been identified [45].

Some insight into the mechanisms involved in the formation of the  $(\sqrt{3} \times \sqrt{3})R30^\circ$  substitutional structures can be obtained by consideration of the activation energy barrier for the phase transition. This activation energy barrier is related to the transition temperature through the Arrhenius equation. For the kick-out mechanism, the transition state could be considered as corresponding to a configuration involving, the alkali metal atom plus an Al atom, over a vacancy in the Al(111) surface. This transition state geometry will yield a



corresponding activation energy barrier (and transition temperature) which *depends* on the species of alkali metal adsorbate since the alkali metal atom is involved in the geometry of the transition state. It may happen, however, that the barrier height is small or comparable to that of an “intermediate geometry” corresponding to that in which the alkali metal atom is in the vacancy (adsorbed substitutionally) and the ejected Al atom in an isolated position on the surface, not yet re-bonded at a kink site at a step. In this case the activation energy barrier (and transition temperature) could be determined using this intermediate geometry. This has been assumed in earlier work to estimate transition temperatures [29,32]. On the other hand, for the mechanism where we consider the possibility that Al atoms desorb from steps to regions *between* on-surface alkali metal atoms, the rate-determining process is likely to be the desorption of Al atoms from the steps. This mechanism will be largely *independent* of the species of the on-surface alkali metal adatoms and correspondingly so will the activation energy barrier and transition temperature be. Interestingly, from HRCLS [35,45] and second harmonic generation measurements [46], it is found that the transition temperature *does* depend on the adsorbate and is higher for Rb than for K, reflecting a higher activation energy barrier for Rb: For Rb the transition temperature was reported to be 250 K [45] and for K temperatures of 220 K [35] and 210 K [46] were given. The fact that the transition temperature does depend on the particular species of the alkali metal atom lends support to the kick-out process. Additional support comes from the STM study [40] in which small Al plateaus on the  $(\sqrt{3} \times \sqrt{3})R30^\circ$  surface, not typically found on the clean surface, were identified. Discussion along similar lines has been presented in some detail in Ref. [29].

We now consider formation of the higher coverage  $(2 \times 2)$  phase. The atomic composition of this phase reveals that another interesting mechanism could be active: On first consideration it would appear that no mass transport of Al atoms is required in its creation, that is, the “missing” Al atoms from the vacancy-layer are seemingly re-bonded between the two Na layers (see Fig. 1). However, because the  $(2 \times 2)$  structure can be formed by adsorption of one-sixth of a monolayer of Na onto the  $(\sqrt{3} \times \sqrt{3})R30^\circ$  structure, in which every third

surface Al atom is *missing*, a reverse process is implied, namely, diffusion of one-third of a monolayer of Al atoms back from kink sites at steps and reaction with the Na atoms to form the  $(2 \times 2)$  phase. A simplistic illustration of this process is provided in Fig. 2. In the STM study [40] “holes” in terraces were observed to have formed on creation of the  $(2 \times 2)$  phase. The number of Al atoms taken from these “holes”, however, was reported to correspond to only  $1/12$  of a monolayer, i.e., less than the required  $1/3$  of a monolayer. This suggests that the additional Al atoms come from steps or that they have undergone long range mass transport and come from areas on the surface not imaged.

We now turn to the second and quite different adsorption system of O on Ru (0001).

### III. O ON RU (0001)

From recent experiments of the catalytic oxidation of carbon monoxide performed at high gas partial pressures, evidence has been presented that Ru (0001) can support an unusually high concentration of oxygen at the surface [47,48]. This is particularly interesting because it is well known that under ultra high vacuum conditions (UHV) the saturation coverage is close to  $\Theta = 1/2$  [49] and very little in fact is actually known about possible structures that may form under high  $O_2$  pressures. In order to investigate the structure and stability of high coverage oxygen structures, we performed density functional theory calculations for various O-adlayers on Ru (0001) as well as for clean Ru (0001), as reported in Ref. [22]. The structures investigated were the two ordered phases,  $(2 \times 2)$  [50] and  $(2 \times 1)$  [51], which form at room temperature under UHV conditions for coverages  $\Theta = 1/4$  and  $\Theta = 1/2$ , respectively, and for several higher coverage  $(1 \times 1)$  structures with coverage  $\Theta = 1$ . The calculations for the  $(2 \times 2)$  and  $(2 \times 1)$  phases provided a test of the accuracy of the calculations through comparison with available LEED intensity analyses. From the comparisons it was found that very good agreement with respect to the preferred adsorption site and the structural parameters was obtained. The investigation for the higher coverage structures revealed that although a  $(1 \times 1)$  phase is not observed to form under UHV conditions using molecular

oxygen, the adsorption of oxygen on Ru(0001) with a  $(1 \times 1)$  structure is appreciably exothermic indicating that it should be able to form. This furthermore implies that its formation at low  $O_2$  pressures is prohibited by kinetic limitations due to activation energy barriers for dissociation.

### A. The $(2 \times 2)$ -O and $(2 \times 1)$ -O phases on Ru (0001)

For the  $(2 \times 2)$  structure, the theoretically obtained binding energy of O relative to the free O atom, in the hcp-hollow site was found to be considerably more favorable than in the fcc-hollow site where the energies are 5.55 eV and 5.12 eV, respectively. For the free O atom, we included the spin polarization energy which is calculated to be 1.521 eV [52]. The DFT-GGA result is in accord with the LEED intensity determination of the hcp-hollow adsorption site for oxygen in this phase. The theoretical O-Ru bond length is 2.10 Å and the first Ru-Ru interlayer spacing is found to be contracted by 2.7 % with respect to the bulk value (using the centers of gravity of the first and second buckled Ru layers). The corresponding LEED-derived values are 2.03 Å and 2.1 %, respectively. As noted above, the calculated bond length is somewhat longer than the experimental one. Lateral and vertical relaxations of the first two Ru layers are induced by the O adatoms, the direction and magnitude of which are well reproduced by the theory (see Ref. [22] for a comparison). Figure 3 shows the atomic geometry of the  $(2 \times 2)$ -O/Ru(0001) structure as determined by the calculations. It can be seen that the three Ru atoms coordinated to the O adatom move laterally away from it resulting in three Ru atoms in the first layer moving closer together; the fourth Ru atom does not move laterally (it is prohibited by symmetry ) but it is vertically displaced in towards the bulk and slightly further than the other three Ru atoms. Similarly in the second Ru layer, three Ru atoms move laterally towards each other and the fourth Ru atom, below the O adatom, is vertically displaced in towards the bulk relative to the other three Ru atoms in the same layer.

Calculations for the  $(2 \times 1)$  structure show that the obtained difference in binding energy

for oxygen in the fcc- and hcp-hollow sites is notably less than for that of the lower coverage ( $2 \times 2$ ) structure; the binding energy of O in the hcp-hollow site is 5.28 eV and that for the fcc-hollow site is 5.00 eV, a difference of 0.28 eV as compared to 0.43 eV. Again, adsorption in the hcp-hollow site is preferred, in agreement with the site determined from the LEED intensity analysis [51]. The oxygen-induced substrate relaxations are particularly complex: the O atoms adsorb in “off” hcp-hollow sites, i.e., they are displaced slightly from the center of the site towards an on-top site, and “row-pairing” and buckling of the first two substrate layers occur. Figure 4 depicts the atomic structure as obtained from the calculations. On comparison with the LEED determined structural parameters (see Ref. [22]) we find that the DFT-GGA calculations predicted all of these relaxations with the one exception that our results indicated row-pairing of the Ru atoms in the *second* Ru layer, as well as in the first layer, and the LEED intensity analysis did not. Both DFT-GGA and LEED find that the first two Ru-Ru interlayer spacings, defined with respect to the centers of gravity of the buckled atomic layers, correspond to the bulk value to within 0.01 Å. The two theoretical O-Ru bond lengths in the ( $2 \times 1$ ) structure, each of approximately 2.08 Å, are very similar to that for the lower coverage structure which was 2.10 Å. The value is again slightly larger than that obtained from the LEED intensity analysis, which for this structure, was 2.02 Å.

### B. The ( $1 \times 1$ )-O/Ru (0001) phase

In view of the very good agreement of the results of the DFT-GGA calculations and the LEED intensity analyses as outlined above, various higher coverage ( $1 \times 1$ )-O structures with coverage  $\Theta = 1$  were investigated. In particular, adlayers with O in the fcc-, and hcp-hollow sites were considered. Similarly to the lower coverage structures, the hcp-hollow site was found to be energetically more favorable than the fcc-hollow site with respective binding energies of 4.84 eV and 4.76 eV; the difference in binding energy of 0.08 eV between the two sites again being reduced as compared to those of the lower coverage structures. Calculations were also performed with a higher energy cut-off and a larger  $\mathbf{k}$ -point set, namely, 60 Ry

and fourteen special  $\mathbf{k}$ -points is the irreducible part of the Brillouin zone. The resulting binding energies differed by only 0.03 eV and by 0.05 eV for the hcp- and fcc-hollow sites, respectively, and the resulting structural parameters differed by not more than 0.02 Å and by 0.04 Å for the hcp- and fcc-hollow sites, respectively, for the two different basis sets. These results are collected in Tab. II. In addition, using the larger basis set, the binding energy of O in the on-top and bridge sites was calculated. These sites were found to be considerably less favorable than the two hollow sites. The obtained binding energies being 3.62, 3.93, 4.81, and 4.87 eV, for the on-top, bridge, fcc- and hcp-hollow sites, respectively. For the hcp-hollow site, the theoretical O-Ru bond length of 2.03 Å is slightly shorter than that of the lower coverage structures (compare 2.10 Å and 2.08 Å for the  $(2 \times 2)$  and  $(2 \times 1)$  structures, respectively) and the first Ru-Ru interlayer spacing is found to be *expanded* by  $\sim 2.7\%$  relative to the bulk spacing. The surface atomic geometry is depicted in Fig. 5.

The value of 4.87 eV for the binding energy of O in the hcp-hollow site on Ru(0001) indicates that the  $(1 \times 1)$  adlayer structure should be able to form because it is considerably larger (by  $\sim 1.8$  eV) than that which the O atoms have in O<sub>2</sub>. As noted above, under UHV conditions using O<sub>2</sub> the saturation coverage is  $\approx 0.5$  associated with the ordered  $(2 \times 1)$  superstructure. Thus, the reason that a  $(1 \times 1)$  adlayer with coverage  $\Theta = 1$  does not form under UHV conditions is apparently due to a kinetic hindering for the dissociation of O<sub>2</sub>. It is probable that such a hindering may be overcome at high O<sub>2</sub> pressures and elevated temperatures as used in the catalytic reactor experiments [47,48] due to the high attempt frequency. Alternatively, if *atomic* oxygen is offered, the  $(1 \times 1)$ -O structure may be realized as we predicted in Ref. [22].

The coverage dependence of the binding energy described above, in which it becomes less favorable with increasing coverage, reflects a repulsive interaction between the adsorbates and implies that no island formation is expected to occur in the coverage regime of  $\Theta = 1/4$  to  $\Theta = 1$ . Concomitantly, the difference in binding energy between the fcc- and hcp-hollow sites becomes less with increasing coverage. In fact, for the full monolayer this difference is quite small. However, because the full monolayer is reached successively via the other

(lower coverage) phases, for which the hcp-hollow site is clearly favored, we expect a nearly perfect hcp-hollow site occupation, i.e. only few fcc-hollow site dislocation structures, for the  $(1 \times 1)$  oxygen layer. In the coverage range investigated, the work function increases with increasing coverage in accordance with the high electronegativity of oxygen and in good agreement with experiment [49]. For the  $(1 \times 1)$ -O structure, the value of the work function change is about 1.11 eV.

Because the  $(1 \times 1)$ -O adlayer is appreciably exothermic it prompts the consideration of whether an even higher coverage of oxygen can adsorb at the surface. To investigate this possibility we performed calculations for three structures with an O coverage of  $\Theta = 1.25$ . These structures are shown in Fig. 6. In the first structure, depicted in Fig. 6a, there are four O atoms in hcp-hollow sites in the  $(2 \times 2)$  surface unit cell and one in an fcc-hollow site. This structure was found to be unstable in that the oxygen atom in the fcc-hollow site did not form a bond with the substrate and lifts off the surface. In the second geometry considered, illustrated in Fig. 6b, an O<sub>2</sub> dimer is adsorbed in the hcp-hollow site of the surface unit cell with the molecular axis perpendicular to the surface. In the remaining three hcp-hollow sites, O atoms are positioned. Likewise, this structure was also found to be unstable. These results indicate that the optimum coverage chemisorbed *on the surface* is  $\Theta=1$ . In the last structure considered, as shown in Fig. 6c, there are four O atoms in hcp-hollow sites in the surface unit cell and one O atom in an octahedral (subsurface) site between the first and second Ru layers. This structure was found to be metastable where the average adsorption energy per O atom in the surface unit cell is 4.09 eV; alternatively stated, a free O atom gains 1.07 eV if it can adsorb in the subsurface octahedral site of the O-covered surface. This geometry is, however, less favorable (by an average of 0.37 eV per atom) than that with four O atoms in hcp-hollow sites and the fifth O atom in an O<sub>2</sub> dimer in gas-phase. That is, while O adsorption under the O-covered surface in an octahedral site is metastable with respect to free O atoms, if O<sub>2</sub> is used, it is energetically more favorable to retain the  $(1 \times 1)$  adlayer structure with the additional O atom in the O<sub>2</sub> dimer in the gas-phase. If, however, atomic oxygen is used it is possible that the oxygen atoms may enter

the subsurface region, provided they can overcome the diffusion energy barrier for passing through the first Ru layer.

#### IV. CONCLUSION

Using density functional theory calculations it has been possible to identify new and unexpected adsorbate phases, as well as obtaining insight into the behavior of the adsorption systems in general. In the present paper this was demonstrated for the  $(2 \times 2)$ -Na phase on Al(111) which represents a binary “four-layer” surface alloy that is able to form even though the constituent atoms are immiscible in bulk, and for the adsorption of oxygen on Ru(0001) for which it was found that a  $(1 \times 1)$ -O adlayer structure should be able to form. As indicated in the introduction, the application of similar theoretical approaches to those mentioned in the present paper, to studies into the interaction and chemical reaction of atoms and molecules at surfaces is expected to be a particularly active area due to the relevance of these processes in heterogeneous catalysis.

#### Acknowledgements

Valuable discussions with M. Scheffler and K. Kambe are gratefully acknowledged.

## REFERENCES

- [1] See for example, G. Pacchioni, P. S. Bagus, and F. Parmigiani (Eds.), *Cluster Models for Surface and Bulk Phenomena*, NATO ASI Ser. Physics, Vol. 283 Plenum Press, New York, 1992.
- [2] For example, the pseudopotential method, M. Scheffler, in *Festkörperproblem* **22** ed. P. Grosse, Vieweg, Braunschweig 1982, p. 115; M. J. Gillan, *J. Phys.: Condens. Matter* **1**, 689 (1989); J. Dabrowski and M. Scheffler, *Phys. Rev. B* **40**, 10391 (1989); J. L. A. Alves, J. Hebenstreit, and M. Scheffler, *Phys. Rev. B* **44**, 6188 (1991); M. C. Payne, H. P. Teter, D. C. Allan, T. A. Arias, J. D. Joannopoulos, *Rev. Mod. Phys.* **69**, 1045 (1992); the linear augmented plane wave (LAPW) method, E. Wimmer, H. Krakauer, M. Weinert, and A. J. Freeman, *Phys. Rev. B* **24**, 864 (1981); M. Weinert, W. Wimmer, A. J. Freeman, and H. Krakauer, *Phys. Rev. Lett.* **47**, 705 (1981); the linear muffin-tin orbital (LMTO) and augmented spherical wave (ASW) method, M. Said, F. Máca, K. Kambe, and M. Scheffler, *Phys. Rev. B* **38**, 8505 (1988); M. Methfessel, D. Hennig, and M. Scheffler, *Phys. Rev. B* **46**, 4816 (1992).
- [3] J. A. White, M. Bird, M. C. Payne, and I. Stich, *Phys. Rev. Lett.* **73**, 1404 (1994).
- [4] B. Hammer, M. Scheffler, K. W. Jacobsen, and J. K. Nørskov, *Phys. Rev. Lett.* **73**, 1400 (1994).
- [5] B. Hammer and M. Scheffler, *Phys. Rev. Lett.* **74**, 3487 (1995).
- [6] E. Pehlke and M. Scheffler, *Phys. Rev. Lett.* **74**, 952 (1995).
- [7] P. Kratzer, B. Hammer, J. K. Nørskov, *Chem. Phys. Lett.* **229**, 645 (1994).
- [8] S. Wilke and M. Scheffler, *Surf. Sci.* **329**, L605 (1991) and *Phys. Rev. B* to appear April 1996.
- [9] A. D. Becke, *J. Chem. Phys.* **96**, 2155 (1992); **97**, 9173 (1992).



- [10] L. Fan and T. Ziegler, *J. Am. Chem. Soc.* **114**, 10890 (1992).
- [11] J. P. Perdew, J. A. Chevary, S. H. Vosko, K. A. Jackson, M. R. Pederson, D. J. Singh, and C. Fiolhais, *Phys. Rev. B* **46**, 6671 (1992).
- [12] B. G. Johnson, C. A. Gonzales, P. M. W. Gill, and J. A. Pople, *Chem. Phys. Lett.* **221**, 100 (1994).
- [13] A. Garcia, C. Elsasser, J. Zhu, S. G. Louie, and M. L. Cohen, *Phys. Rev. B* **46**, 9829 (1992).
- [14] P. H. T. Philipsen, G. te Velde, and E. J. Baerends, *Chem. Phys. Lett.* **226**, 583 (1994).
- [15] P. Hu, D. A. King, S. Crampin, M.-H. Lee, and M. C. Payne, *Chem. Phys. Lett.* **230**, 501 (1994).
- [16] C. Lee, D. Vanderbilt, K. Laasonen, R. Car, and M. Parrinello, *Phys. Rev. B* **47**, 4863 (1993).
- [17] N. Moll, M. Bockstedte, M. Fuchs, E. Pehlke, and M. Scheffler, *Phys. Rev. B* **52**, 2550 (1995).
- [18] D. R. Hamann, *Phys. Rev. Lett.* **76**, 660 (1996).
- [19] B. G. Johnson, P. M. W. Gil, and J. A. Pople, *J. Chem. Phys.* **98**, 5612 (1993).
- [20] C. Stampfl and M. Scheffler, *Surf. Sci.* **319**, L23 (1994).
- [21] J. Burchhardt, M. M. Nielsen, D. L. Adams, E. Lundgren, J. N. Andersen, C. Stampfl, M. Scheffler, A. Schmalz, S. Aminpirooz, and J. Haase, *Phys. Rev. Lett.* **74**, 1617 (1995).
- [22] C. Stampfl and M. Scheffler, *Phys. Rev. B*, in press.
- [23] J. Neugebauer and M. Scheffler, *Phys. Rev. B* **46**, 16067 (1992).
- [24] R. Stumpf and M. Scheffler, *Comp. Phys. Commun.* **79**, 447 (1994).

- [25] D. M. Ceperley and B. I. Alder, Phys. Rev. Lett. **45**, 556 (1980); P. Perdew and A. Zunger, Phys. Rev. B **23**, 5048 (1981).
- [26] S. G. Louie, S. Froyen, and M. L. Cohen, Phys. Rev. B **26**, 1738 (1982).
- [27] C. Stampfl and M. Scheffler; J. N. Andersen; R. Fasel and J. Osterwalder; R. D. Diehl and R. McGrath; H. Over, H. Bludau, M. Gierer, and G. Ertl; Surf. Rev. Lett. **2**, 317 (1995),
- [28] *Physics and Chemistry of Alkali Metal Adsorption*, edited by H. P. Bonzel, A. M. Bradshaw, and G. Ertl (Elsevier, Amsterdam, 1989).
- [29] D. L. Adams, Proceedings of the Annual Meeting of the German Physical Society, Berlin, March 1995, Applied Physics.
- [30] A. Schmalz, S. Aminpirooz, L. Becker, J. Haase, J. Neugebauer, M. Scheffler, D. R. Batchelor, D. L. Adams, and E. Bøgh, Phys. Rev. Lett. **67**, 2163 (1991).
- [31] M. M. Nielsen, J. Burchhardt, D. L. Adams, E. Lundgren, and J. N. Andersen, Phys. Rev. B **50**, 4718 (1994).
- [32] C. Stampfl, J. Burchhardt, M. Nielsen, D. L. Adams, M. Scheffler, H. Over and W. Moritz, Phys. Rev. Lett. **69**, 1532 (1992).
- [33] M. M. Nielsen, J. Burchhardt, D. L. Adams, E. Lundgren and J. N. Andersen, Phys. Rev. Lett. **72**, 3370 (1994).
- [34] T. Nagao, Y. Iizuka, M. Umeuchi, T. Shimazaki, and C. Oshima, Surf. Sci. **329**, 269 (1995).
- [35] J. N. Andersen, E. Lundgren, R. Nyholm and M. Qvarford, Surf. Sci. **289**, 307 (1993).
- [36] J. O. Porteus, Surf. Sci. **41**, 515 (1974).
- [37] A. Hohlfeld and K. Horn, Surf. Sci. **211/212**, 844 (1989).

- [38] J. N. Andersen, M. Qvarford, R. Nyholm, J. F. van Acker, and E. Lundgren, Phys. Rev. Lett. **68**, 94 (1992).
- [39] M. Kerkar, D. Fisher, D. P. Woodruff, R. G. Jones, R. D. Diehl and B. Cowie, Surf. Sci. **278**, 246 (1992).
- [40] H. Brune, J. Wintterlin, R. J. Behm, and G. Ertl, Phys. Rev. B **51**, 13592 (1995).
- [41] B. Chakraborty and R. W. Siegel, Phys. Rev. B **27** (1983) 4535.
- [42] C. Filippi, D. J. Singh, and C. J. Umrigar, Phys. Rev. B **50**, 14947 (1994).
- [43] Y.-M. Juan, E. Kaxiras, and R. G. Gordon, Phys. Rev. B **51**, 9521 (1995).
- [44] C. Stampfl, unpublished.
- [45] E. Lundgren, R. Nyholm, J. Burchhardt, D. Heskett, and J. N. Andersen, Surf. Sci. **343**, 37 (1995).
- [46] J. Wang, Z. C. Ying, and E. W. Plummer, Phys. Rev. B **51**, 5590 (1995).
- [47] C. H. F. Peden and D. W. Goodman, J. Phys. Chem. **90**, 1360 (1986).
- [48] C. H. F. Peden, D. W. Goodman, M. D. Weisel, and F. M. Hoffmann, Surf. Sci. **253**, 44 (1991).
- [49] L. Surnev, G. Rangelov, and G. Bliznakov, Surf. Sci. **159**, 299 (1985).
- [50] M. Lindroos, H. Pfnür, G. Held and D. Menzel, Surf. Sci. **222**, 451 (1989).
- [51] H. Pfnür, G. Held, M. Lindroos, and D. Menzel, Surf. Sci. **220**, 43 (1989).
- [52] A. P. Seitsonen and M. Fuchs, priv. comm.

TABLES

Interlayer spacing ( $\text{\AA}$ )	$Z(\text{Na}_f\text{-Al}_1)$	$Z(\text{Al}_1\text{-Na}_s)$	$Z(\text{Na}_s\text{-Al}_2)$	$Z(\text{Al}_2\text{-Al}_3)$	$Z(\text{Al}_3\text{-bulk})$
LEED	0.85	0.55	1.52	2.25	2.28
SEXAFS	0.75	0.70	1.50		
DFT-LDA	0.72	0.62	1.46	2.23	2.27
DFT-GGA	0.86	0.49	1.63	2.29	2.33

TABLE I. Interlayer spacings,  $Z$ , between the atomic layers indicated in parenthesis (see Fig. 1). For the rumpled Al layers, five and six, the interlayer distances are given with respect to the center of gravity of the respective layer. In relation to this, we note that in Refs. [20,21], the interlayer spacings for the DFT-LDA results were given with respect to the positions of the three Al atoms per unit cell which have the same vertical position and not with respect to the center of gravity of the rumpled layer.

$(1 \times 1)$ -O/Ru (0001) hcp-hollow site						
	O-Ru	$d_{z,1}$	$d_{z,2}$	$d_{z,3}$	$d_{z,\text{bulk}}$	$E_b$
DFT-GGA (40 Ry)	2.04	1.28	2.27	2.19	2.19	4.84
DFT-GGA (60 Ry)	2.03	1.26	2.24	2.17	2.19	4.87
$(1 \times 1)$ -O/Ru (0001) fcc-hollow site						
DFT-GGA (40 Ry)	2.05	1.29	2.33	2.13	2.19	4.76
DFT-GGA (60 Ry)	2.03	1.27	2.29	2.13	2.19	4.81

TABLE II. Structural parameters for  $(1 \times 1)$ -O/Ru (0001) with O in the hcp- and fcc-hollow sites for the different basis sets (see text). O-Ru,  $d_z$ , and  $E_b$  represent, the O-Ru bond length, the interlayer spacings (in Ångstrom), and binding energy (in eV), respectively.

FIGURES

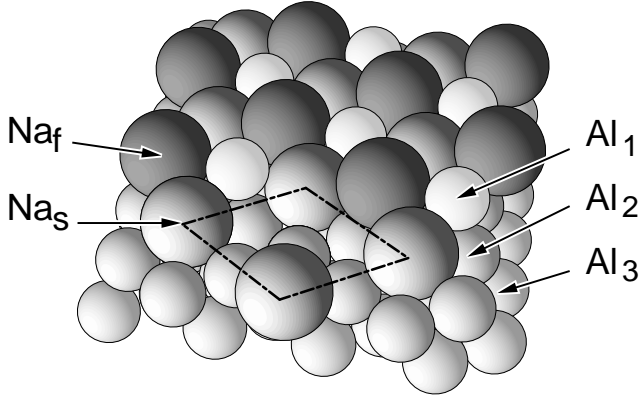


FIG. 1. The atomic structure of  $(2 \times 2)$ -Na/Al(111). Some atoms have been removed to expose the lower layers where the surface unit cell is also drawn.  $\text{Na}_f$  and  $\text{Na}_s$  represent, respectively, the Na atoms in fcc-hollow and substitutional sites and  $\text{Al}_1$  the Al atoms located in hcp-hollow sites, with respect to the vacancy-layer.  $\text{Al}_2$  and  $\text{Al}_3$  represent the Al atoms in the vacancy-layer and in the layer below, respectively.

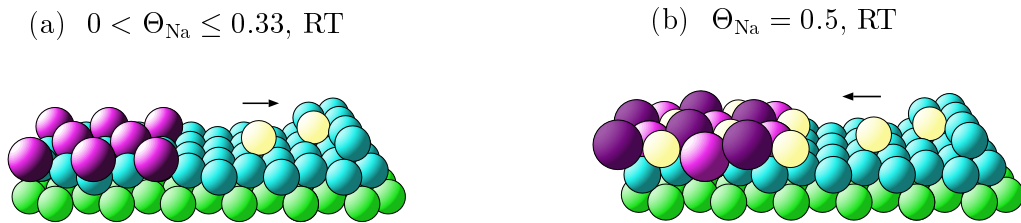


FIG. 2. Possible mass transport mechanism. (a) Island formation occurs [40] with a  $(\sqrt{3} \times \sqrt{3})R30^\circ$  structure with Na atoms in substitutional sites, for coverages  $0 < \Theta_{\text{Na}} \leq 1/3$ : Every third Al atom is “missing”; Al atoms diffuse to steps. (b) Surface alloy formation with a  $(2 \times 2)$  geometry implies diffusion of Al atoms back from steps.

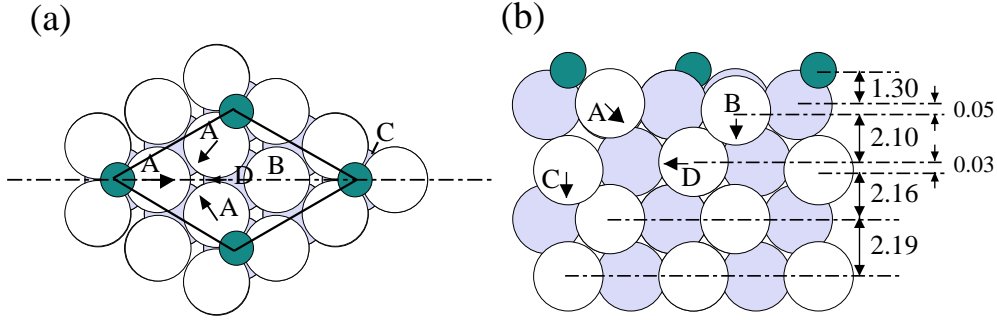


FIG. 3. Top view (a) and side view (b) of the atomic geometry of  $(2 \times 2)$ -O/Ru(0001). The arrows (not drawn to scale) indicate the direction of the displacements of the substrate atoms with respect to the bulk positions. The dashed line in (a) indicates the plane of the cross-section used in (b). Small dark grey circles represent oxygen atoms and large white and grey circles represent Ru atoms, where the latter correspond to those lying in the next plane. Interlayer spacings are given in Ångstrom.

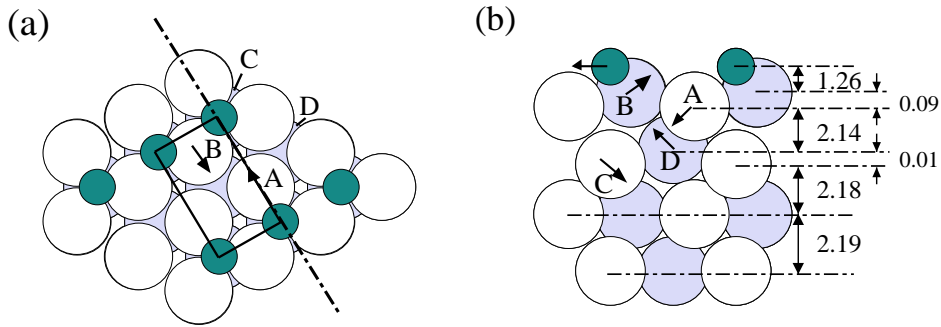


FIG. 4. Top view (a) and side view (b) of the atomic geometry of  $(2 \times 1)$ -O/Ru(0001). The arrows (not drawn to scale) indicate the direction of the atomic displacements. The dashed line in (a) indicates the plane of the cross-section used in (b). Small dark grey circles represent oxygen atoms and large white and grey circles represent Ru atoms, where the latter correspond to those lying in the next plane. Interlayer spacings are given in Ångstrom.

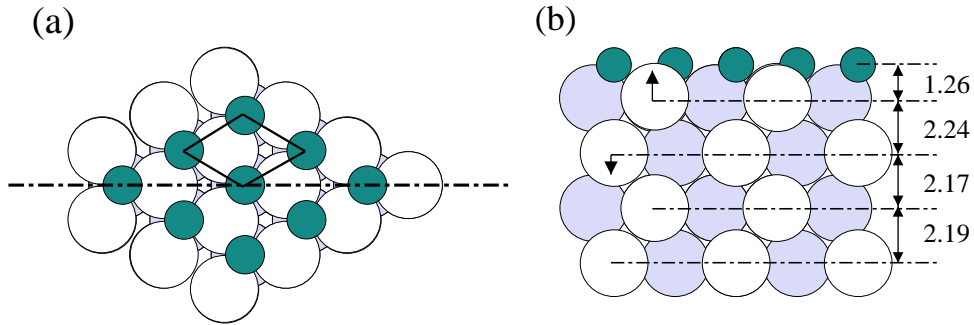


FIG. 5. Top view (a) and side view (b) of the atomic geometry of  $(1 \times 1)$ -O/Ru(0001) with O in the hcp-hollow site (obtained with a 60 Ry cut-off and fourteen special  $\mathbf{k}$ -points in the irreducible part of the Brillouin zone). The arrows (not drawn to scale) indicate the direction of the displacements of the substrate atoms with respect to the bulk positions. Small dark grey circles represent oxygen atoms and large white and grey circles represent Ru atoms, where the latter correspond to those lying in the next plane. Interlayer spacings are given in Ångstrom.

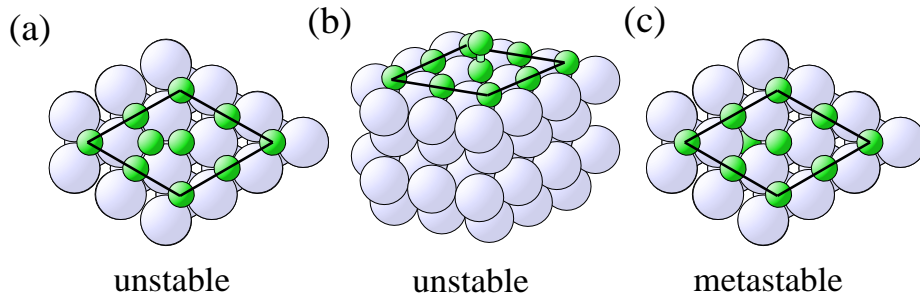


FIG. 6. Structures considered for O on Ru(0001) for a coverage of  $\Theta = 1.25$ . The Ru atoms are depicted as the large circles and the O atoms as the small circles. The surface unit cell is indicated.